Intravascular molecular-structural imaging with a miniaturized integrated near-infrared fluorescence and ultrasound catheter

Stephan Kellnberger[#,1], **Georg Wissmeyer**[#,1], **Mazen Albaghdadi**[1], **Zhonglie Piao**[2], **Wenzhu Li**[1], **Adam Mauskapf**[1], **Philipp Rauschendorfer**[3,4], **Guillermo J. Tearney**[2], **Vasilis Ntziachristos**[3,4], **Farouc A. Jaffer**[1,2,*]

[1]Cardiovascular Research Center, Cardiology Division, Massachusetts General Hospital, Boston, MA 02114

[2]Wellman Center for Photomedicine, Massachusetts General Hospital, Boston, MA 02114

[3]Institute of Biological and Medical Imaging, Helmholtz Zentrum München, Neuherberg, Germany

[4]Chair of Biological Imaging, Central Institute for Translational Cancer Research (TranslaTUM), Technical University of Munich, Germany

[#] These authors contributed equally to this work.

Abstract

Coronary artery disease (CAD) remains a leading cause of mortality and warrants new imaging approaches to better guide clinical care. We report on a miniaturized, hybrid intravascular catheter and imaging system for comprehensive coronary artery imaging in vivo. Our catheter exhibits a total diameter of 1.0 mm (3.0 French), equivalent to standalone clinical intravascular ultrasound (IVUS) catheters but enables simultaneous near-infrared fluorescence (NIRF) and IVUS molecular-structural imaging. We demonstrate NIRF-IVUS imaging in vitro in coronary stents using NIR fluorophores, and compare NIRF signal strengths for prism and ball lens sensor designs in both low and high scattering media. Next, in vivo intravascular imaging in pig coronary arteries demonstrates simultaneous, co-registered molecular-structural imaging of experimental CAD inflammation on IVUS and distance-corrected NIRF images. The obtained results suggest substantiual potenital for the NIRF-IVUS catheter to advance standalone IVUS, and enable comprehensive phenotyping of vascular disease to better assess and treat patients with CAD.

*Correspondence: Farouc Jaffer, MGH Cardiology/Cardiovascular Research Center, 185 Cambridge Street, Boston, USA. fjaffer@mgh.harvard.edu.

Graphical Abstract

Hybrid NIRF-IVUS *in vivo* imaging cross-section of the left anterior descending coronary artery in a swine atherosclerosis model with co-registered plaque inflammation and structural information. NIRF information is encoded in the outer circular colormap and fused with structural information depicting greyscale ultrasound. Scale bar, 1 mm.

Keywords

Intravascular imaging; Intravascular endoscopy; Near-Infrared Imaging; Intravascular Ultrasound

1 | INTRODUCTION

High-resolution intravascular imaging plays a key role in coronary artery disease (CAD) assessment and for guidance of percutaneous coronary intervention. Accordingly, coronary artery imaging necessitates high technological and performance demands for intravascular imaging systems, including small-scaled catheters (1.2 mm diameter, or 3.6 French (Fr)) coupled with fast frame rate imaging, to enable safe and time-efficient clinical operation [1].

Intravascular ultrasound (IVUS), the predominant worldwide intracoronary imaging approach, and optical coherence tomography (OCT), an increasingly used approach, have been widely used for high-resolution cardiovascular disease imaging of atherosclerosis and stents [2]. IVUS allows for deeper imaging up to a centimetre in coronary arteries at rotational speeds of 30 frames s^{-1} with axial and lateral resolutions in the order of 30 μm and pullback speeds of around 1 mm s^{-1} [3,4]. OCT, on the other hand, has superior imaging resolution of ~10 μm with pullback speeds of 40 mm s^{-1} [5], however at the expense of requiring flushing of blood and reduced penetration depth (1–2 mm) due to high light absorption and scattering properties of soft tissue [6]. To advance plaque characterization, new hybrid approaches have integrated fluorescence lifetime imaging (FLIM) with IVUS or

OCT [7,8], or diffuse near-infrared spectroscopy (NIRS) with IVUS [9,10]. FLIM measures the fluorescence emission lifetime characteristic to specific fluorophores and NIRS allows to assess the biochemical composition of coronary plaques.

Recent efforts have focused on high-resolution near-infrared fluorescence (NIRF) molecular imaging for intravascular endoscopy. Integrated NIRF-IVUS molecular-structural imaging can provide a more holistic understanding of the CAD, enabling better diagnosis and therefore improved patient treatment [11–13]. In contrast to NIRS and FLIM, NIRF offers the unique ability to perform molecular imaging using injectable NIRF imaging agents that can report on inflammation, angiogenesis, and osteogenesis, key pathophysiologic markers of vulnerable plaque. The combination of structural imaging with NIRF molecular imaging has yielded new hybrid imaging approaches such as NIRF-OCT and NIRF-IVUS, which have recently demonstrated improved diagnosis of atherosclerosis and stent pathology [14–16]. With the frequent clinical use of IVUS, there is particular interest in advancing the state of intravascular NIRF-IVUS imaging. For example, previously reported first-generation NIRF-IVUS systems employed a side-by-side design of the optical element (prism) and the IVUS transducer [17]. While this design allowed for successful NIRF-IVUS image acquisition, it resulted in bulky total catheter diameters of up to 1.4 mm, too large for routine in vivo coronary artery imaging and future clinical translation. In a recent advance, freeform micro-optics have been presented for FLIM-IVUS, allowing for astigmatism and chromatic dispersion compensation introduced by the catheter sheath and for serial arrangement of optical element and IVUS transducer [18]. However, these streamlined optics have yet to be applied to NIRF-IVUS catheters and imaging systems.

In this work, we present a miniaturized, hybrid NIRF-IVUS imaging catheter which, due to its small outer diameter of 0.55 mm, can readily be integrated into the sheath of a clinical IVUS system with a total outer diameter of 1.0 mm (3.0 Fr). This catheter is facilitated by a sensor design where the optical element and the IVUS transducer are implemented in series at the catheter tip. We further introduce ball lens optical sensors for NIRF-IVUS imaging and compare prism to ball lens catheter designs by assessing their in vitro imaging performance in scattering and absorbing media. Finally, we provide the first demonstration that the miniaturized NIRF-IVUS catheter can assess intracoronary plaque inflammation, by imaging experimental pig arteries in vivo. The developed catheter design, employing a serial arrangement of the optical sensing element and the IVUS transducer, to the best of our knowledge, represents the smallest diameter NIRF-IVUS catheter reported and advances the potential for clinical intravascular NIRF-IVUS imaging.

2 | EXPERIMENTAL

2.1 | Hybrid NIRF-IVUS imaging system

The NIRF-IVUS imaging setup consists of the back-end console and the coronary artery catheters as depicted in Fig. 1(a). The back-end console comprises a 750 nm fiber-coupled laser (B&W Tek, Newark, DE, USA) for dynamic NIRF-signal excitation between 5 – 25 mW, an ultrasound pulser-receiver unit (Model 5073PR, Panametrics, Waltham, MA, USA) operated at 100 V amplitude with 10 kHz pulse repetition frequency, a photomultiplier tube (Model H7422–50, Hamamatsu, Japan) for NIRF-signal detection, and a cage cube system

(Thorlabs, Newton, NJ, USA) containing a dichroic mirror (T770lpxr, Chroma, Bellow Falls, VT, USA) and selected optical bandpass filters (ET845/55m, Chroma, Bellow Falls, VT, USA) to separate the excitation beam from the emission (fluorescent) beam. Throughout the experiments, laser power was adjusted to 12 mW at the catheter tip for both prism and ball lens designs. The motor drive unit (MDU) consists of a customized fiber-optic rotary joint (FORJ) integrated into a slip ring (SR) (Alpha Slip Rings, Austin, TX, USA). The rotation-dependent transmission efficiency of the FORJ is above 95% per revolution. A DC motor (Model 3268G042BX4AES-4096, Faulhaber, Germany) rotates the SR-FORJ with a pulley system at speeds of up to 1,800 rpm. The rotation speed and pullback speed for the presented work were set to 300 rpm and 1 mm s^{-1}, respectively, in order to avoid non-uniform rotational distortion (NURD) artifacts.

The MDU is further mounted on a translational stage (X-LRQ stage, Zaber, Vancouver, BC, Canada) that enables pullback speeds up to 2 mm s^{-1}. Component control as well as signal acquisition and processing are performed on a PC using Python and Matlab (Mathworks, Natick, MA, USA).

The catheter system has been designed to integrate with commercially available and clinically utilized coronary artery catheter systems. Specifically, we engineered the size of our catheter so that it is equal to the size of a contemporary clinical IVUS catheter (Opticross 1.0 mm/3.0 Fr catheter, Boston Scientific Corporation, Marlborough, MA, USA). Our catheter without the sheath exhibited a miniaturized outer diameter of 0.55 mm, enabled by a serial layout of the US and optical sensors as shown in Fig. 1(b). The US sensor consists of a piezoelectric (PZT) element (size: $0.4 \times 0.6 \times 0.25$ mm^3, central frequencies: 40 MHz or 60 MHz; Boston Scientific Corporation, Marlborough, MA, USA) manually soldered to a micro-coaxial cable (Highspeed Int, Scottsdale, AZ, USA). For optical excitation and detection, we first employed an optical prism design (see Fig. 1(c)) as reported previously [15,17], as well as second ball-lens design (see Fig. 1(d)). Ball lenses have been used in intravascular imaging in OCT-catheters [14], enabling light focusing with potential higher fluence into the target vessel wall, simpler manufacturing, and a more robust operation. In contrast to OCT geometries, where the beam-path is perpendicular to the catheter axis in order to maximize penetration depth, the presented ball-lens design has a pre-polish diameter of 360 μm manufactured under a polish angle of 40° in order to overlap the US detection cone with the optical excitation beam path. The increased optical path length due to angulation of the ball lens is negligible in intravascular imaging for distances up to 3 mm between catheter and vessel wall. The geometry of the angled IVUS and NIRF beams for both prism and ball lens designs are illustrated in Fig. 1 (b). In both layouts, the physical offset between the IVUS transducer and the optical element along the catheter axis was around 750 μm and was compensated for during image analysis. The polished surface is then sputter-coated with a thin Au-layer to allow for reflection in aquatic environments and fixated inside the ferrule by epoxy. The full width at half maximum (FWHM) of the prism was measured to be 400 μm for the prism and 270 μm for the ball lens at a distance of 1 mm, respectively. The PZT and the optical element are serially embedded inside a micro-manufactured stainless steel ferrule, micro-welded to a single-layer torque coil with high maximum torque threshold (outer diameter: 0.55 mm; model: Actone, Asahi-Intecc,

Japan) which in turn houses the micro-coaxial cable for IVUS signal transmission, and a 50/105 μm optical fiber (Thorlabs, Newton, NJ, USA) for NIRF signal transmission.

2.2 | *In vitro* and *in vivo* experimental settings

For phantom experiments, we mounted the catheter inside a 3D printed water container and used a flexible tubing (PE50, outer diameter 965 μm, wall thickness 381 μm; Braintree Scientific, Inc., Braintree, MA, USA) filled with different concentrations of AlexaFluor750 (AF750 NIR fluorophore (excitation/emission 749/775nm), Thermo Fisher Scientific, Waltham, MA, USA) or indocyanine green (ICG/IC-green, Akorn, Lake Forest, IL, USA) for NIR fluorescence measurements. A second phantom experiment was performed to compare the NIRF imaging quality of the miniaturized catheter to previous designs. For these experiments, we immersed a coronary stent in ICG (concentration: 500 nM) for 1 minute, rendering the stent fluorescent in the NIR. Standalone complementary IVUS images were obtained with a commercially available IVUS system and catheter (Opticross and iLab, Boston Scientific, Marlborough, MA, USA) for NIRF-IVUS image comparison.

In vivo studies were performed on an institutional (Massachusetts General Hospital) animal care and use committee (IACUC) protocol. One Yorkshire pig (male, 44 kg) underwent hyperlipidemic feeding for 2 weeks (Research Diets Inc., New Brunswick NJ, USA). To induce atherosclerosis, the pig was anesthetized with xylazine/telazol (at 2.2/4.4 mg/kg) and intubated. Next, femoral arterial access was obtained, and the left coronary artery was selected with an HS guide. Then a cutting balloon (3.0×10 mm, Wolverine, Boston Scientific, Marlborough, MA, USA) was utilized to injure the arterial intima and accelerate atherosclerosis development in the mid left anterior descending (LAD) artery at 1:1 ratio, using standalone IVUS guidance. Finally, a 2.75×12 mm bare metal stent was placed in the LAD distal to the area of cutting balloon injury. Hyperlipidemic diet feeding was continued. Four weeks later, the animal received an IV injection of ProSense 750 (VM110, PerkinElmer, Waltham, MA, USA), a NIRF molecular imaging agent activated by inflammatory cathepsin proteases [14], at a dose of 1.4 mg/kg i.v.. The next day, the animal returned to the cardiac catheterization laboratory for intravital NIRF-IVUS and standalone IVUS imaging.

3 | RESULTS AND DISCUSSION

3.1 | Optical sensor design and distance correction

In a first step, the ball lens design was compared to prism-based catheter designs in model calculations and in vitro measurements. Similar to the model for light transmission in diffusive media as shown in [17], we applied two different correction algorithms for low scattering and diffuse media: For water, we used the Beer-Lambert law to correct for distance dependent light attenuation and in blood, we applied the Twersky model [19] to evaluate the light transmission (parameters: prism B = 13.000; q = 2.100; / ball lens B = 15.000; q = 2.310).

For the corresponding in vitro experiments, we performed pullbacks for the four variations of ball lens and prism optics in the media water and rabbit blood, respectively. The tubing

phantom was filled with a 100 nM concentration of the NIR fluorophore AF750 and the increasing distance between sensor-head and phantom was recorded by the IVUS modality.

Fig. 2(a) shows the comparison of calculated and measured NIRF signals. The goodness-of-fit was found to be excellent, with corresponding R2 values between model and experimental data ranging from R2 = 0.92 to R2 = 0.98. We found that both the ball lens and the prism designs have similar light transmission in water and blood with correlation coefficients of >0.98. In water, the resulting distance correction could be applied up to 2 mm distance with an SNR of 9.3 dB in the uncorrected image. In blood, the distance correction could be applied up to 0.3 mm distance with an SNR of 5.3 dB in the uncorrected image. We note that light transmission in diffuse media and for relevant distances was found to be similar for both prism and ball lens catheters. As a consequence, we opted for ball lens catheters in all following experiments, as these optics are simpler to manufacture and represent a more precise and robust design, inter alia due to the absence of adhesives.

Next, we evaluated the accuracy of the computed Twersky model with a ball lens pullback of an AF750 tubing phantom (100 nM). The tubing was fixed to the catheter at an offset angle of less than 30° to enable varying distances with increasing pullback length relative to the catheter. Fig. 2(b) shows the results of the pullback obtained over a distance of 26 mm with a pullback speed of 1 mm s^{-1}. The distance between catheter and phantom was highest with 1.6 mm at the beginning of the pullback and zero at the crossing at 15 mm pullback distance. The non-distance corrected NIRF map shows attenuating NIRF signals with increasing distance from the catheter (Fig. 2(b)) and unquantified NIRF signal intensities. After applying distance correction, we restored the concentration of the fluorophore with a homogenous NIRF signal distribution over the entire pullback (see Fig. 2(b)).

The experiment was then repeated with the same AF750 tubing NIRF phantom as above but was performed in freshly obtained rabbit blood placed at room temperature. Fig. 2(c) shows the pullback over a distance of 16 mm with a pullback speed of 1 mm s^{-1}. Compared to Fig. 2(b), the non-distance corrected image shows a more rapid light attenuation across the pullback. Applying the Twersky model, we reconstructed a homogenous distribution of the tubing with a calculated NIRF concentration of 100 nM which corresponded to the fluorophore concentration embedded inside the tubing. Here, the strong light absorption and -scatter in blood, limited the effective sensing depth to distances < 0.3 mm from the catheter.

3.2 | *In vitro* stent validation

Next, we tested the distance correction algorithm on a NIR fluorophore-coated coronary stent submerged in water. We imaged a coronary stent (Xience V 2.5 × 23mm drug-eluting stent, Abbott Laboratories, Abbott Park, Il, USA) that was immersed in indocyanine green (ICG) of a concentration of 500 nM for 1 minute. The pullback was then performed across the entire length of the stent with a pullback speed of 1 mm s^{-1}. Fig. 2(d) shows the reconstructed IVUS image of the stent along with the distance corrected NIRF map. A close-up view of the NIRF image (Fig. 2(d), bott. inset) visualizes several crossing single stent struts with the overlays of representative full width half maxima (FWHM) of stent struts with 238 μm and 280 μm, respectively. Here, the SNR in the distance corrected image was calculated to be 37 dB (uncorrected: 32 dB). The combined cross-sectional NIRF-IVUS

image (Fig. 2(d), top inset) depicts the stent struts in the IVUS image as well as the quantified and distance corrected NIRF signals, which are co-located to the stent struts.

3.3 | Intracoronary NIRF-IVUS imaging of plaque inflammation

In a final step, we tested the catheter in vivo in a pig model of coronary atherosclerosis, a model recapitulating several aspects of human CAD. A male Yorkshire pig with atherosclerosis in the LAD artery underwent i.v. ProSense VM110 injection to sense inflammatory cathepsin protease activity, and then 1 day later, underwent NIRF-IVUS and standalone IVUS intracoronary imaging.

The acquired NIRF map is shown in Fig. 3 and exhibited focal NIRF signal at a pullback distance of around 38 mm with a SNR of 13.6 dB. Accordingly, two representative cross sections were then selected away from and within the NIRF signal hotspot as indicated by C1 (green arrow) and C2 (red arrow), respectively. The corresponding superimposed NIRF-IVUS cross sections with the raw and distance-corrected NIRF signal are depicted in rows C1 and C2, respectively. Standalone IVUS images of the LAD corresponding to the respective NIRF-IVUS cross-sectional slices (tolerance ~3 mm) with mild atherosclerosis (intimal thickening indicated by blue arrows) confirm the presence of inflamed plaque and are consistent with the acquired NIRF-IVUS images. Co-registration between the new NIRF-IVUS system and the commercial standalone IVUS device was performed with fiducials including side branches and an implanted 2.75×12mm bare metal coronary stent in the LAD, which was imaged by both catheter systems.

3.4 | Discussion

Two NIRF-IVUS catheter designs with different NIRF-optical sensing technologies have been implemented and tested. The prism design and the ball lens design show similar imaging performance in scattering and absorbing media. Although the ball lens enables optical focusing and a potentially higher fluence compared to the unfocused prism design, we found that operating the ball lens in scattering and absorbing media significantly impedes its focusing effect, resulting in similar NIRF signal intensities as obtained with the prisms. In contrast to NIRF-IVUS, NIRF-OCT runs in a scattering free environment due to blood purging, thereby capitalizing on the full potential of the focusing ability of the ball lens. Nevertheless, the ball lens design enabled a more robust operation of the catheter and has a favourable adhesive-free manufacture method.

Validation of this catheter design with combined distance correction *in vivo* in a coronary atherosclerosis pig model demonstrated quantified signal reconstruction and plaque detection. This result was further confirmed by standalone IVUS and demonstrated NIRF-IVUS detection of coronary plaque inflammation for the first time. By detecting NIRF signals through blood in phantom and in vivo experiments, we demonstrated that NIRF-IVUS imaging is feasible without flushing, while contrast/saline flushing is mandatory for NIRF-OCT imaging.

4 | CONCLUSION

In this Letter, we present a novel miniaturized 3.0F hybrid NIRF-IVUS catheter engineered for simultaneous molecular-structural imaging of intravascular coronary arteries in living subjects. Due to the smaller size, our catheter can be seamlessly integrated into a commercially available catheter sheath, and thus enable flushing and tracking of the catheter with radiopaque markers on x-ray fluoroscopy. While both NIRF-IVUS and NIRF-OCT offer simultaneous molecular structural imaging of CAD, coupling NIRF with IVUS offers several advantages compared to coupling NIRF with OCT. First, IVUS is the predominant clinical intravascular imaging approach used worldwide. Second, IVUS does not require blood flushing with contrast, allowing safer procedures with less risk to the patient. Third, coronary IVUS has greater depth penetration than OCT (5–8 mm vs. 1–2 mm) and thus can assess full coronary wall thickness and plaque burden, where OCT fails due to the lower penetration of photons through soft tissue.

Further preclinical large animal studies are testing the 1.0 mm NIRF-IVUS catheter to assess atheroma plaque biology and stent healing in vivo, and to more accurately predict plaque progression and stent complications. Subsequent efforts will focus on clinical translation of the NIRF-IVUS catheter for first-in-human intracoronary imaging trials and utilizing translatable NIRF targeted imaging agents such as ICG [20]. In terms of catheter development, we presented a crucial engineering step towards miniaturization and subsequent clinical translation by the serial arrangement of the optical sensor and the IVUS transducer. New catheter designs and system improvements are planned to enable stable catheter mechanics and reduce NURD artifacts. Next generation catheters will be made of dual layer torque coils, lower autofluorescence dual-clad fibers [14], and ultrasound pulsers with higher pulse repetition rate. In combination with a more robust pullback stage these improvements will enable higher rotation speeds to enhance clinical translation. Strategies to overcome tissue motion e.g. by ECG-triggered gating, can particularly help to improve IVUS image acquisition in future [21]. As blood absorption currently limits intravascular NIRF sensing to about 1 mm through blood [17], additional efforts to improve fluorescence sensitivity utilizing optical fibers with higher numerical aperture are being explored. The utilization of dual clad fibers with low autofluorescence will further improve sensitivity to detect NIR fluorophores beyond the current effective sensing depth of 0.3 mm. Furthermore, we are currently developing a new distance correction algorithm with automatic IVUS image segmentation of the vessel wall, coronary artery plaque, and stent struts, to expedite distance correction for NIRF signal analysis.

DATA AVAILABILITY STATEMENT

The data that support the findings of this study are available on request from the corresponding author. The data are not publicly available due to privacy or ethical restrictions.

ACKNOWLEDGMENTS

REFERENCES

1. Kuku KO, Singh M, Ozaki Y, Dan K, Chezar-Azerrad C, Waksman R, and Garcia-Garcia HM, Front. cardiovasc. med2020, 7, 107. [PubMed: 32695796]

2. Buccheri S, Franchina G, Romano S, Puglisi S, Venuti G, D'Arrigo P, Francaviglia B, Scalia M, Condorelli A, Barbanti M, Capranzano P, Tamburino C, and Capodanno D, JACC Cardiovasc. Interv2017, 10, 2488. [PubMed: 29153502]

3. V Bourantas C, Jaffer FA, Gijsen FJ, van Soest G, Madden SP, Courtney BK, Fard AM, Tenekecioglu E, Zeng Y, van der Steen AFW, Emelianov S, Muller J, Stone PH, Marcu L, Tearney GJ, and Serruys PW, Eur. Heart J2017, 38, 400. [PubMed: 27118197]

4. Garcia-Garcia HM, Costa MA, and Serruys PW, Eur. Heart J2010, 31, 2456. [PubMed: 20823109]

5. Ughi GJ, Wang H, Gerbaud E, Gardecki JA, Fard AM, Hamidi E, Vacas-Jacques P, Rosenberg M, Jaffer FA, and Tearney GJ, JACC. Cardiovasc. Imaging2016, 9, 1304. [PubMed: 26971006]

6. Ntziachristos V, Nat. Methods2010, 7, 603. [PubMed: 20676081]

7. Bec J, Phipps JE, Gorpas D, Ma D, Fatakdawala H, Margulies KB, Southard JA, and Marcu L, Sci. Rep2017, 7, 1. [PubMed: 28127051]

8. Lee MW, Song JW, Kang WJ, Nam HS, Kim TS, Kim S, Oh WY, Kim JW, and Yoo H, Sci. Rep2018, 8, 1. [PubMed: 29311619]

9. Waksman R, Di Mario C, Torguson R, Ali ZA, Singh V, Skinner WH, Artis AK, Ten Cate T, Powers E, Kim C, Regar E, Wong SC, Lewis S, Wykrzykowska J, Dube S, Kazziha S, van der Ent M, Shah P, Craig PE, Zou Q, Kolm P, Brewer HB, Garcia-Garcia HM, Samady H, Tobis J, Zainea M, Leimbach W, Lee D, Lalonde T, Skinner W, Villa A, Liberman H, Younis G, de Silva R, Diaz M, Tami L, Hodgson J, Raveendran G, Goswami N, Arias J, Lovitz L, Carida II R, Potluri S, Prati F, Erglis A, Pop A, McEntegart M, Hudec M, Rangasetty U, and Newby D, Lancet2019, 394, 1629. [PubMed: 31570255]

10. Gardner CM, Tan H, Hull EL, Lisauskas JB, Sum ST, Meese TM, Jiang C, Madden SP, Caplan JD, Burke AP, Virmani R, Goldstein J, and Muller JE, JACC Cardiovasc. Imaging2008, 1, 638. [PubMed: 19356494]

11. Jaffer FA and Verjans JW, Heart 2014, 100, 1469. [PubMed: 24365664]

12. Bourantas CV, Garcia-Garcia HM, Naka KK, Sakellarios A, Athanasiou L, Fotiadis DI, Michalis LK, and Serruys PW, J. Am. Coll. Cardiol2013, 61, 1369. [PubMed: 23500282]

13. Marcu L, J. Biomed. Opt2010, 15, 011106. [PubMed: 20210432]

14. Yoo H, Kim JW, Shishkov M, Namati E, Morse T, Shubochkin R, McCarthy JR, Ntziachristos V, Bouma BE, Jaffer FA, and Tearney GJ, Nat. Med2011, 17, 1680. [PubMed: 22057345]

15. Abran M, Stähli BE, Merlet N, Mihalache-Avram T, Mecteau M, Rhéaume E, Busseuil D, Tardif J, and Lesage F, Biomed. Opt. Express2015, 6, 3989. [PubMed: 26504648]

16. Li Y, Jing J, Qu Y, Miao Y, Zhang B, Ma T, Yu M, Zhou Q, and Chen Z, Biomed. Opt. Express2017, 8, 1036. [PubMed: 28271001]

17. Bozhko D, Osborn EA, Rosenthal A, Verjans JW, Hara T, Kellnberger S, Wissmeyer G, Ovsepian SV, McCarthy JR, Mauskapf A, Stein AF, Jaffer FA, and Ntziachristos V, Eur. Hear. J. - Cardiovasc. Imaging2017, 18, 1253.

18. Bec J, Li C, and Marcu L, Opt. Lett2019, 44, 4961. [PubMed: 31613239]

19. Twersky V, J. Opt. Soc. Am1970, 60, 1084. [PubMed: 5480400]

20. Verjans JW, Osborn EA, Ughi GJ, Calfon Press MA, Hamidi E, Antoniadis AP, Papafaklis MI, Conrad MF, Libby P, Stone PH, Cambria RP, Tearney GJ, and Jaffer FA, JACC-Cardiovasc. Imag2016, 9, 9.

21. Von Birgelen C, Mintz GS, Nicosia A, Foley DP, Van Der Giessen WJ, Bruining N, Airiian SG, Roelandt JRTC, De Feyter PJ, and Serruys PW, J. Am. Coll. Cardiol1997, 30, 436. [PubMed: 9247516]
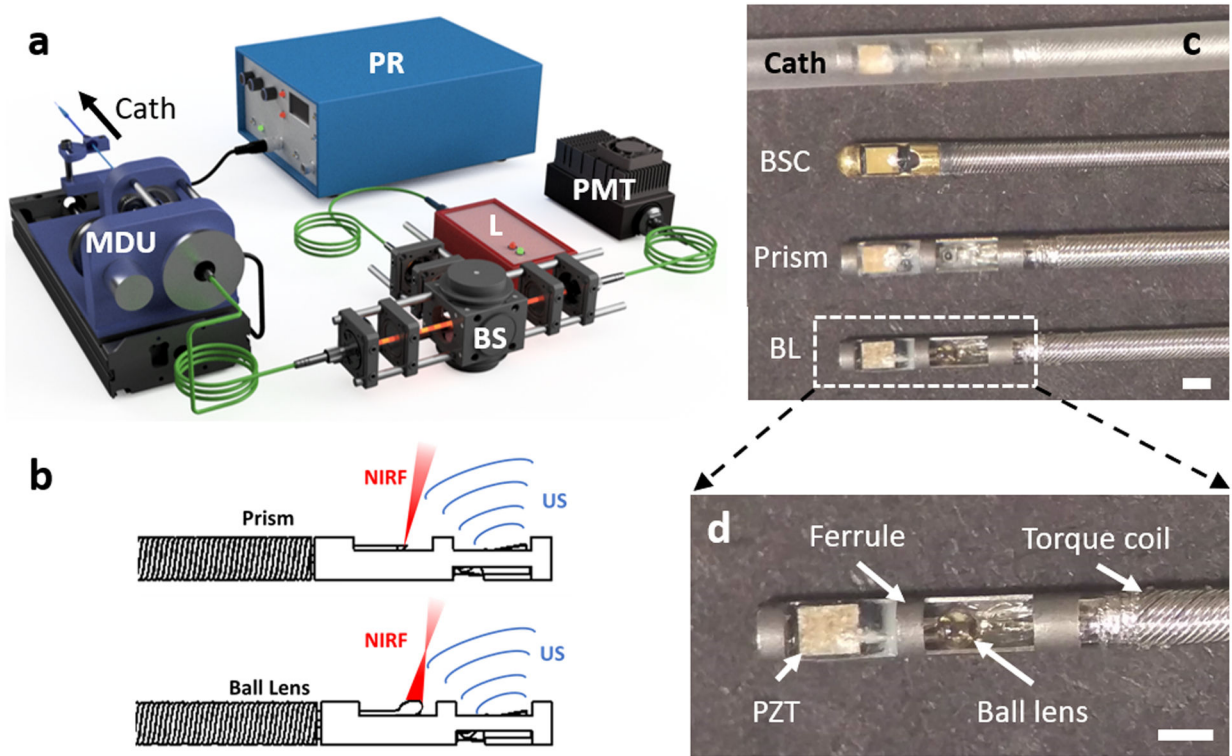
Figure 1.
Hybrid intravascular near-infrared fluorescence (NIRF) and intravascular ultrasound (IVUS) imaging system. A, Schematic of the read-out system. BS, beam splitter; Cath, catheter sheath; L, excitation laser; MDU, motor drive unit; PMT, photomultiplier tube; PR, pulse receiver. B, Illustration of the NIRF and ultrasound (US) beam paths of prism and ball lens catheter design. Angled beam paths minimize axial offset during image acquisition. C, Comparison of commercial and novel catheter designs. BSC, Boston Scientific Opticross 3F catheter; Prism, hybrid NIRF-IVUS catheter with prism optics; BL, hybrid NIRF-IVUS catheter with ball lens optics. Scale bar, 500 μm. D, Close-up view and itemization of ball lens catheter. PZT, piezoelectric element. Scale bar, 500 μm
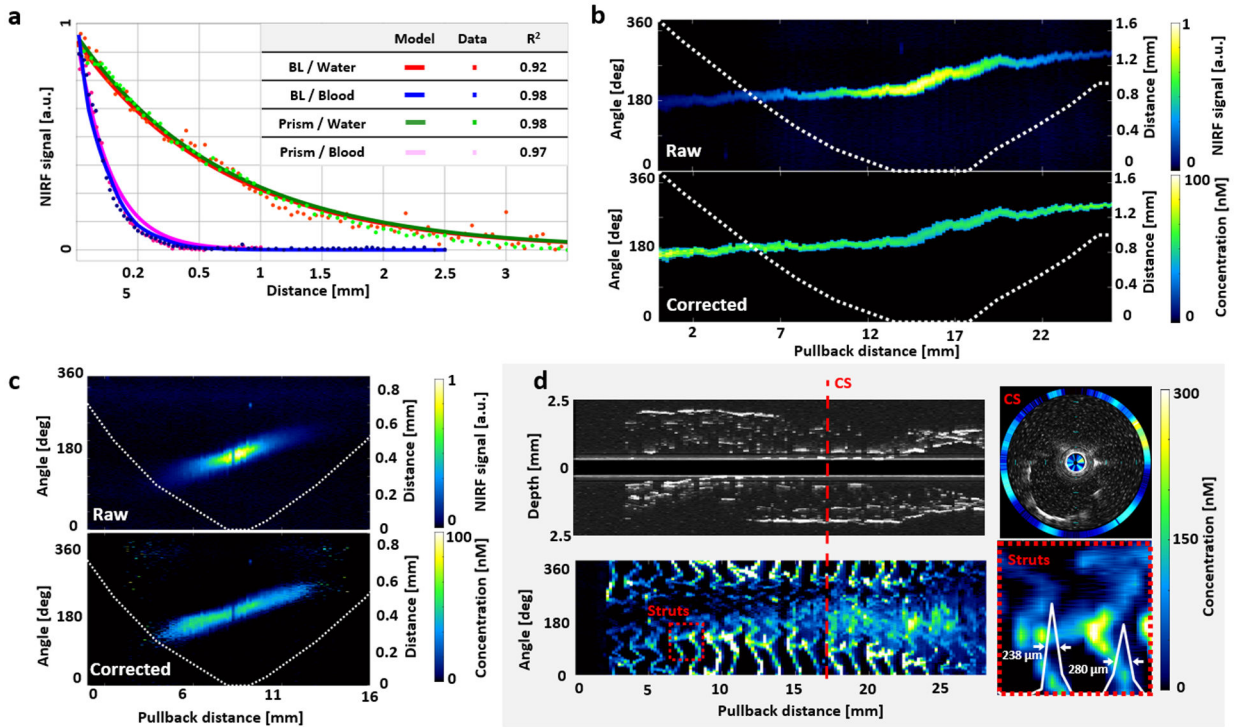
Figure 2.
Hybrid NIRF-IVUS in vitro image acquisition. A, Comparison of modeled and measured NIRF signal for prism and ball lens (BL) based catheter designs in water and blood with corresponding R2 values. NIRF measurement performed on 100 nM AF750 phantom in PE tubing. B,C, BL catheter pullback across AF750 tubing in water, B, and blood, C, with raw and distance-corrected NIRF data, respectively. Phantoms identical to, A. Distance to sensor is indicated on the second y-axis represented by the white dotted line. D, Hybrid imaging of ICG coated coronary stent with longitudinal IVUS image and corresponding NIRF image. IVUS aspect ratio 2:1. Cross section (CS) indicated by dashed line and arranged with superimposed NIRF and IVUS data. Two stent struts indicated by dotted square with corresponding close-up and respective FWHM
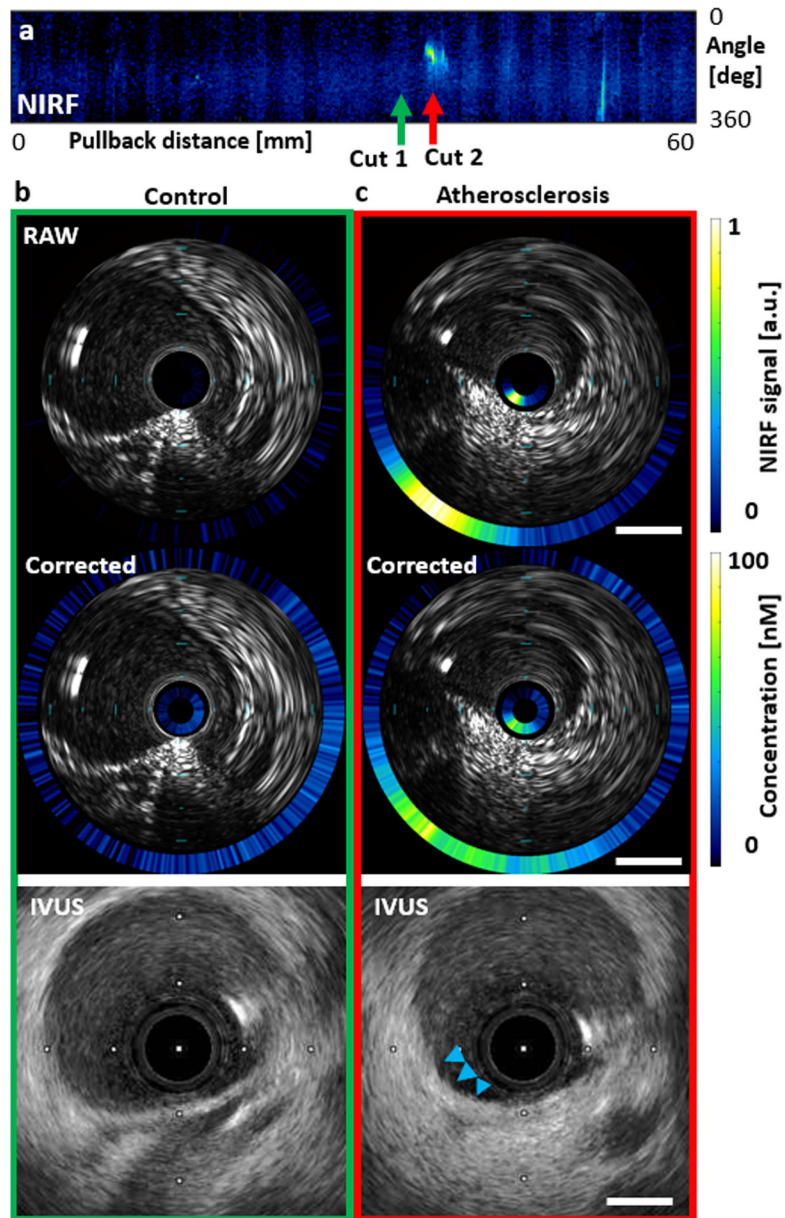
Figure 3.
Hybrid NIRF-IVUS in vivo imaging of a swine atherosclerosis model. NIRF image over 60 mm pullback in the left anterior descending artery. Arrows at Cut 1 (green) and Cut 2 (red) indicate pullback positions of control and atherosclerotic cross-sections, depicted in rows B and C, respectively. Superimposed NIRF and IVUS data before and after distance correction. Corresponding IVUS images recorded with commercial 60 MHz catheters and blue arrows indicating atherosclerosis. Scale bar, 1 mm